

A 500–750 GHz RF MEMS Waveguide Switch

Umer Shah, *Member, IEEE*, Theodore Reck, *Senior Member, IEEE*, Henrik Frid, *Student Member, IEEE*, Cecile Jung-Kubiak, *Member, IEEE*, Goutam Chattopadhyay, *Fellow, IEEE*, Imran Mehdi, *Fellow, IEEE*, and Joachim Oberhammer, *Senior Member, IEEE*

Abstract—This paper reports on a submillimeter-wave 500–750 GHz microelectromechanical systems (MEMS) waveguide switch based on a MEMS-reconfigurable surface to block/unblock the wave propagation through the waveguide. In the non-blocking state, the electromagnetic wave can pass freely through the MEMS-reconfigurable surface, while in the blocking state, the electric field lines of the TE_{10} mode are short-circuited that blocks the wave propagation through a WM-380 (WR-1.5) waveguide. A detailed design parameter study is carried out to determine the best combination of the number of horizontal bars and vertical columns of the MEMS-reconfigurable surface for achieving a low insertion loss in the non-blocking state and a high isolation in the blocking state for the 500–750 GHz band. Two different switch concepts relying either on an ohmic-contact or a capacitive-contact between the contact cantilevers have been implemented. The measurements of the switch prototypes show a superior RF performance of the capacitive-contact switch. The measured isolation of the capacitive-contact switch designed with an 8 μm contact overlap is 19–24 dB and the measured insertion loss in the non-blocking state is 2.5–3 dB from 500 to 750 GHz including a 400 μm long micromachined waveguide section. By measuring reference chips, it is shown that the MEMS-reconfigurable surface contributes only to 0.5–1 dB of the insertion loss, while the rest is attributed to the limited sidewall metal thickness and to the surface roughness of the 400 μm long micromachined waveguide section. Finally, reliability measurements in an uncontrolled laboratory environment on a comb-drive actuator with an actuation voltage of 28 V showed no degradation in the functioning of the actuator over one hundred million cycles. The actuator was also kept in the actuated state for ten days and showed no sign of failure or deterioration.

Index Terms—Micromachined waveguide, rectangular waveguide, RF microelectromechanical systems (MEMS), submillimeter-wave, terahertz, waveguide switch.

I. INTRODUCTION

WAVEGUIDES exhibit a very low insertion loss and a high power handling capability, which makes them

Manuscript received November 7, 2016; accepted February 6, 2017. The contribution of KTH was supported in part by the European Research Council Consolidator Grant 616846, in part under The Swedish Foundation for Strategic Research Synergy Grant Electronics SE13-007, and in part under a Nils and Hans Backmark scholarship.

U. Shah, H. Frid, and J. Oberhammer are with the Department of Micro and Nanosystems, School of Electrical Engineering, KTH Royal Institute of Technology, Stockholm SE-100 44, Sweden (e-mail: umers@kth.se; hfrid@kth.se; joachimo@kth.se).

T. Reck, C. Jung-Kubiak, G. Chattopadhyay, and I. Mehdi are with the Jet Propulsion Laboratory, California Institute of Technology, Pasadena, CA 91109 USA (e-mail: Theodore.reck@jpl.nasa.gov; Cecile.D.Jung@jpl.nasa.gov; goutam.chattopadhyay@jpl.nasa.gov; imran.mehdi@jpl.nasa.gov).

Color versions of one or more of the figures in this paper are available online at <http://ieeexplore.ieee.org>.

Digital Object Identifier 10.1109/TTHZ.2017.2670259

the preferred transmission media for high-frequency and high-power applications. Rectangular waveguides are the most commonly used waveguide type at millimeter- and submillimeter-wave frequencies. These waveguides are usually fabricated from metals utilizing conventional metal machining techniques. However, for waveguides at WM-380 (WR-1.5) band and above, the typically specified fabrication accuracy is 15–20 μm [1], making the fabrication more difficult, costly, and time consuming [2]. The dimensional accuracy requirements are even more severe for resonant structures [1]. As an alternative, micromachining can be employed to fabricate waveguides for submillimeter-wave frequency using silicon, which is then metallized [3]. Silicon micromachined waveguides have already shown encouraging results, fabricated for applications at 2.7 THz [4].

Microwave waveguide switches are used in waveguide-based front-ends for signal routing, signal control, frequency band selection, beam scanning, and calibration and redundancy applications. Conventional waveguide switch technology is mainly based on two concepts, namely, the mechanical switch concept using rotary motors and the semiconductor switch concept using p-i-n diodes and MESFETS integrated into the waveguide. The mechanical switches exhibit low insertion loss and high isolation but are bulky, heavy, require high power, and have a very slow switching speed [5]. On the other hand, semiconductor switches are small in size and have a fast switching speed but exhibit poor insertion loss and isolation, especially at higher frequencies [6]. Microelectromechanical systems (MEMS) switches fabricated by micromachining have the potential to combine the advantages of both the mechanical and the semiconductor switches and replace the existing switch technology. This is due to the fact that the RF MEMS switches offer very low insertion loss, high isolation, high linearity, large bandwidth of operation, low power consumption, switching speed in microsecond range, and high miniaturization [7]. These switches have evolved and matured since their inception in the early 1990s and by now the major challenges they are facing are power handling and reliability [8]. At high input power levels, the power handling is limited by two mechanisms, namely, the self-actuation in the open state and the latching in the closed state [9]. At submillimeter-wave frequencies, power handling is not an issue since at these frequencies only a few milliwatts power is typically available [10]. Reliability, on the other hand, is limited by dielectric charging for capacitive switches and by the contact physics for metal-contact microswitches [11]. In recent publications [12], [13], layered contacts have been used to enhance reliability of metal contact switches by having a soft metal coated with a thin layer of a hard metal.

MEMS waveguide switches utilizing a ridge waveguide with electrothermal and electrostatic actuators have previously been reported for Ku and K band applications [14], [15]. More recently, an upper V-band waveguide switch design based on curled up MEMS actuators integrated inside the waveguide channel [16] has been shown, achieving a better than 20 dB isolation and good insertion loss performance. Furthermore, the authors have previously shown a very low insertion loss (below 0.3 dB) and a very high isolation (above 30 dB) MEMS waveguide switch for the upper V-band using a MEMS-reconfigurable surface to block the wave propagation in a rectangular waveguide [17], [18]. In a recent publication, the authors have used these MEMS-reconfigurable surfaces for switching waveguide stubs to implement a phase shifter operating in the frequency band between 500 and 550 GHz [19], which was the highest frequency RF MEMS device ever reported so far.

This paper introduces the first ever submillimeter-wave MEMS waveguide switch operating in the frequency band between 500 and 750 GHz using a MEMS-reconfigurable surface [17], [18] to block/unblock the wave propagation. This MEMS reconfigurable surface waveguide switch concept is very broadband, as the bandwidth is only limited by the waveguide-modes cutoff. The authors have reported, in a recent conference publication [20], the basic concept of this MEMS waveguide switch at WM-380 (WR-1.5) frequencies. This paper is an extension of the conference publication and discusses the switch design in detail and present new measurement data (both electromechanical and RF). To the best knowledge of the authors, the RF MEMS switch reported here is the first RF MEMS switch above 220 GHz [21] and the first MEMS waveguide switch above 75 GHz. Very recently, another MEMS waveguide switch operating between 500 and 750 GHz based on a ridge waveguide using an electrostatic actuator was reported [22] and our conference publication [20] was referenced as the first MEMS waveguide switch at these frequencies by that paper.

II. CONCEPT AND DESIGN

The waveguide switch reported in this paper comprises a single-pole single-throw design utilizing a MEMS-reconfigurable surface inserted in the cross-sectional plane of the rectangular waveguide as shown in Fig. 1. The use of the MEMS-reconfigurable surface for blocking/unblocking the wave propagation into a waveguide has already been shown by Baghchehsaraei *et al.* [17] and Baghchehsaraei and Oberhammer [18] for V-band. Fig. 1(b) shows the two states of the MEMS waveguide switch. In the non-blocking state, the gap between the contact cantilevers allows for the electromagnetic wave to propagate freely through the MEMS-reconfigurable surface and in the blocking state, the movable contact cantilevers are moved to contact the fixed contact cantilevers to form a series of vertical columns which short circuit the electric field lines of the TE_{10} mode blocking the electromagnetic wave propagation.

The overall switch performance is influenced by the number of horizontal bars (rows), the number of vertical contact cantilevers (columns), and the overlap of the contact cantilevers. The performance variation based on these model parameters are simulated using full-wave simulations in CST

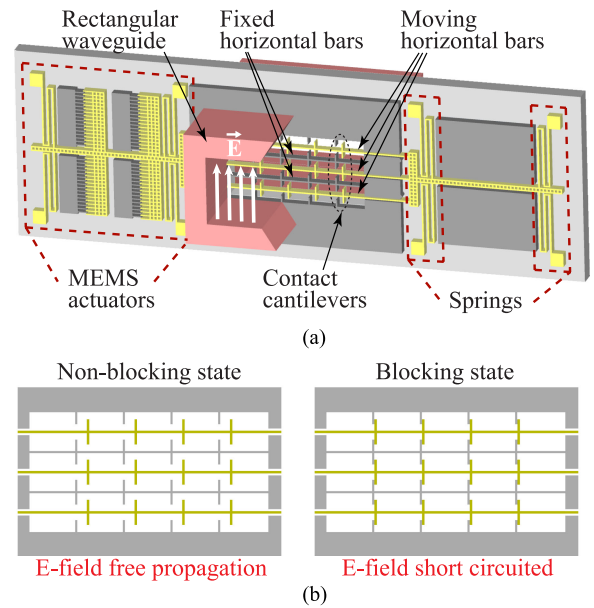


Fig. 1. Submillimeter-wave MEMS waveguide switch design using a MEMS-reconfigurable surface: (a) 3-D illustration of the cross section and (b) non-blocking and blocking state of the MEMS waveguide switch.

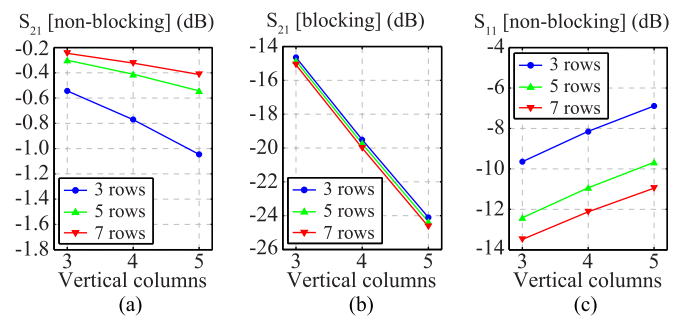


Fig. 2. Design parameter study at 625 GHz for an ohmic-contact overlap of $2 \mu\text{m}$: (a) insertion loss in the non-blocking state, (b) isolation in the blocking state, and (c) return loss in the non-blocking state.

Microwave Studio and are shown in Figs. 2 and 3 to find the best combination of the model parameters for the switch design for 500–750 GHz, i.e., ten times higher frequency than previous designs. The simulation results show that the isolation in the blocking state improves, while the insertion loss in the non-blocking state degrades with increasing number of vertical columns (see Figs. 2 and 3). The number of horizontal bars has a minimal impact on the isolation performance in the blocking state since the horizontal bars are perpendicular to the short-circuited electric field lines. In the non-blocking state of the switch, the insertion loss is significantly higher when three horizontal bars are used instead of four or five horizontal bars. This is an indirect effect resulting from the larger contact cantilever length used for a switch design with lower number of horizontal bars to maintain the same contact overlap. The longer contact cantilevers adversely affect the waveguide electric field lines in the non-blocking state since the contact cantilevers are parallel to the field lines. The degradation of the insertion loss with increasing length of the

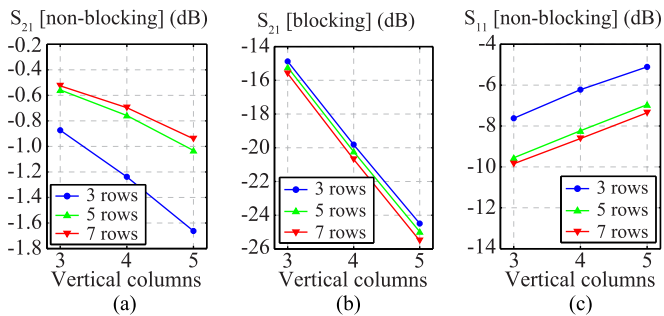


Fig. 3. Design parameter study at 625 GHz for an ohmic-contact overlap of $8\ \mu\text{m}$: (a) insertion loss in the non-blocking state, (b) isolation in the blocking state, and (c) return loss in the non-blocking state.

contact cantilevers is also observed when the contact overlap is increased from 2 to $8\ \mu\text{m}$ as shown in Figs. 2(a) and 3(a), respectively. This design parameter study makes it clear that for the optimal switch design, the selection of the number of horizontal bars and vertical columns requires a compromise between insertion loss, isolation, and the return loss. Based on the simulation results, the design with seven horizontal bars and four vertical columns is selected for a $2\ \mu\text{m}$ contact overlap since it has the non-blocking state insertion and return loss below $0.4\ \text{dB}$ and $12\ \text{dB}$, respectively, and the blocking state isolation above $20\ \text{dB}$.

It has been shown by the authors in a recent publication [19] that due to fabrication inaccuracies, an ohmic contact cannot be guaranteed for all individual switch contacts simultaneously. For the design with $2\ \mu\text{m}$ contact overlap, each contact cantilever has a length of $11\ \mu\text{m}$ with a $4\ \mu\text{m}$ width resulting in a spring constant of $60\ 900\ \text{N/m}$, which limits the possible movement of all further cantilevers into contact to only $0.5\ \text{nm}$ after the first contact is closed. Thus, with the implemented actuator design, closing of all further switch contacts is not guaranteed. In contrast, the spring constant of the contact cantilevers for the V-band ohmic-contact MEMS waveguide switch design published previously by the authors was only $170\ \text{N/m}$ [17], [18], which is much more compliant and allows for a possible further movement of $200\ \text{nm}$ after the first contact is closed. To overcome this issue, the contact overlap was increased from 2 to $8\ \mu\text{m}$. This results in the required isolation being achieved in the blocking state even for a small air gap between the contact cantilevers, i.e., a capacitive contact is sufficient and a metal contact is not required. This increased overlap adversely influences the non-blocking state return loss as shown in Figs. 2(c) and 3(c), which is a design compromise. Therefore, a second switch design, herein referred to as capacitive-contact waveguide switch in contrast to the $2\ \mu\text{m}$ overlap ohmic-contact switch, with the $8\ \mu\text{m}$ contact overlap using five horizontal bars and four vertical columns achieving a simulated insertion loss below $0.8\ \text{dB}$, isolation above $20\ \text{dB}$ and the return loss below $8\ \text{dB}$ was also fabricated.

Moreover, the authors have shown in the previous V-band waveguide switch publication [18] that a strong sinusoidal configuration of the contact cantilevers in the waveguide cross section achieves a similar overall performance for a reduced number of contact points. For the current WM-380 (WR-1.5) wave-

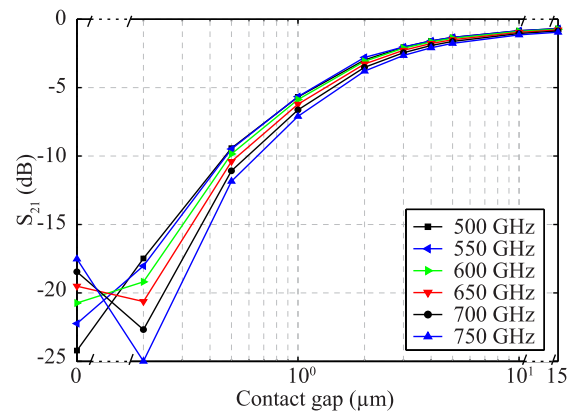


Fig. 4. Simulation results of the design parameter study to evaluate the switch isolation when having a capacitive contact instead of an ohmic contact for a contact overlap of $8\ \mu\text{m}$ using five horizontal bars and four vertical columns.

guide switch design, the waveguide dimensions are such that the design with the maximum number of contact cantilevers only has a total of 24 contact points instead of 440 contact points used in [18]. Any further reduction in this number of contact points is not possible while simultaneously maintaining similar performance of the blocking state isolation and non-blocking state insertion and return loss.

Fig. 4 shows S_{21} as a function of the contact gap for a switch design with the $8\ \mu\text{m}$ contact overlap using five horizontal bars and four vertical columns. The desired isolation is achieved even for a contact gap of $200\ \text{nm}$ when the overlap between the contact cantilevers is $8\ \mu\text{m}$. This gap is used in further simulations in this paper to better model the contact between the contact cantilevers in the blocking state. Furthermore, a $15\ \mu\text{m}$ initial contact gap was chosen for the non-blocking state.

The MEMS switch has standard WM-380 (WR-1.5) rectangular waveguide dimensions ($0.380\ \text{mm} \times 0.190\ \text{mm}$) with the electrostatic comb-drive MEMS actuator having 160 fingers placed on one side of the narrow wall of the waveguide using four folded-beam springs as suspension beams each with a length of $700\ \mu\text{m}$, symmetrically placed around the narrow wall of the waveguide opening. Four different comb-drive designs with different spring widths and finger gaps achieving spring constant variations of 1.06 , 1.69 , and $3.59\ \text{N/m}$ were implemented as actuator variations.

III. FABRICATION AND ASSEMBLY

The assembled switch consists of a MEMS waveguide switch chip with the MEMS-reconfigurable surface and a top silicon chip that is used to align the MEMS waveguide switch chip to the waveguide flanges. The MEMS waveguide switch chips are fabricated using a silicon-on-insulator (SOI) wafer in a two mask micromachining process developed by Baghchehsaraei *et al.* [17] and Baghchehsaraei and Oberhammer [18]. The fabricated chips are metallized by sputtering a gold layer thickness of $700\ \text{nm}$ on the SOI handle wafer and a gold layer thickness of $200\ \text{nm}$ on the SOI device layer. Fig. 5 illustrates a close-up SEM image of a single MEMS waveguide switch chip showing the MEMS-reconfigurable surface, the comb-drive actuators,

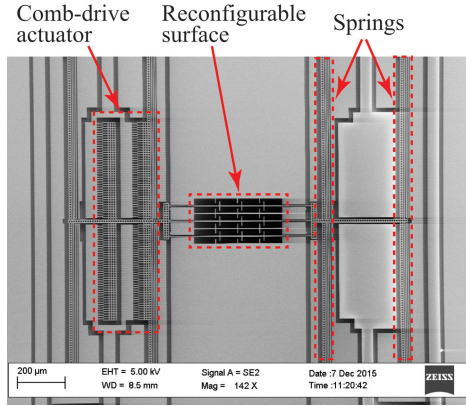


Fig. 5. Close-up SEM image of the fabricated MEMS waveguide switch chip with MEMS-reconfigurable surface and the comb-drive actuators.

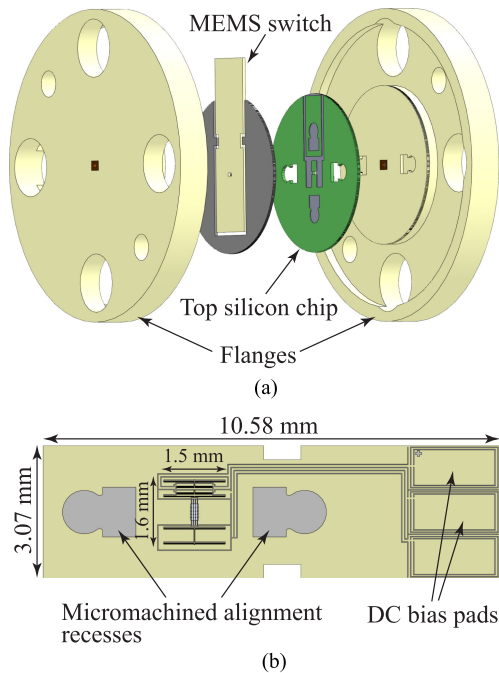


Fig. 6. MEMS waveguide switch: (a) exploded-view drawing showing the mounting/assembly of the MEMS waveguide switch into the WR-1.5 waveguide flanges, and (b) illustration of the complete MEMS waveguide switch chip.

and the mechanical springs. The total dimensions of the MEMS waveguide switch elements are $1.6 \text{ mm} \times 1.5 \text{ mm}$. The processed wafer had a total of 112 MEMS waveguide switch chips achieving a process yield of between 90% and 95% during fabrication in a university classroom.

Fig. 6(a) shows the exploded-view drawing illustrating the mounting/assembly procedure of the MEMS waveguide switch and (b) shows a drawing of the entire MEMS waveguide switch chip of overall dimensions of $3.07 \text{ mm} \times 10.58 \text{ mm}$, including the dc bias lines, bias pads, and alignment recesses. The waveguide flanges, the MEMS waveguide switch chip, and the top silicon chip have omega-shaped alignment recesses where omega-shaped springs are inserted for accurate alignment between the metal and the silicon pieces [23]. Fig. 7 shows microscope pictures of the mounting/assembling of the MEMS wave-

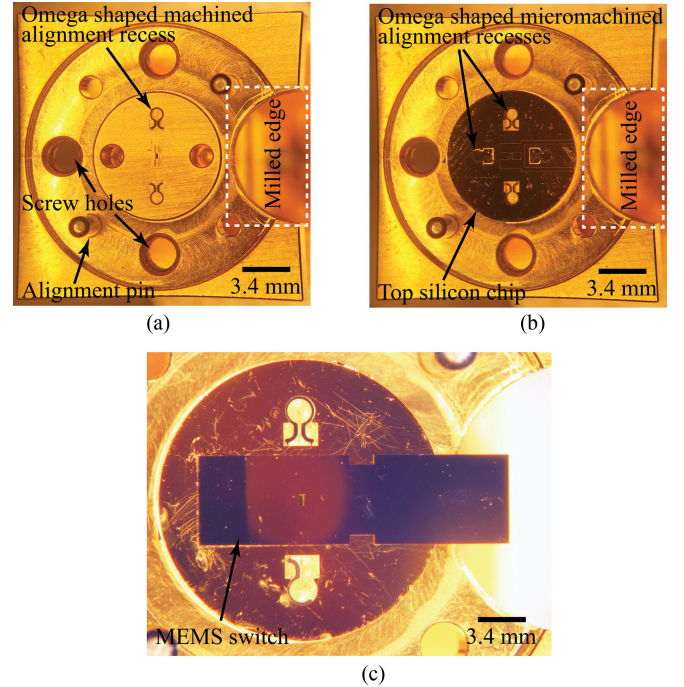


Fig. 7. Assembly/mounting of the MEMS waveguide switch: (a) waveguide flange with omega springs inserted into the omega-shaped micromachined alignment recesses, (b) placement of the top silicon chip, and (c) placement of the MEMS waveguide switch chip.

guide switch. First, omega-shaped silicon springs are placed in the machined alignment recesses on the waveguide flange [see Fig. 7(a)]. This is followed by alignment and placement of the top silicon chip on the waveguide flange [see Fig. 7(b)]. Next, omega-shaped silicon springs are placed in the etched micro-machined alignment recesses on the top silicon chip and the MEMS waveguide switch chip is aligned and placed on the top of the top silicon chip [see Fig. 7(c)]. Finally, the second waveguide flange is placed on top and the whole assembly is screwed together. One of the waveguide flanges has an edge removed on one side (see Fig. 7) so that the dc bias pads on the MEMS waveguide switch chip can be accessed by dc probes.

IV. CHARACTERIZATION AND ANALYSIS

A. Submillimeter-Wave Characterization

The submillimeter-wave measurements of the MEMS waveguide switch prototypes were performed with an Agilent PNA-X system using VDI WR1.5 (WM-380)-VNAX Extenders calibrated using SOLT calibration. Two different MEMS waveguide switch concepts have been implemented: 1) capacitive-contact switch with a contact overlap of $8 \mu\text{m}$ for which capacitive, i.e., proximity, contact between the cantilevers is sufficient and 2) an ohmic-contact switch with a contact overlap of $2 \mu\text{m}$ relying on metal contact between the cantilevers, i.e., physical touching of all contact points and sufficiently low contact resistance.

1) *Capacitive-Contact Switch*: Fig. 8 shows the simulated and measured insertion and return loss for the capacitive-contact

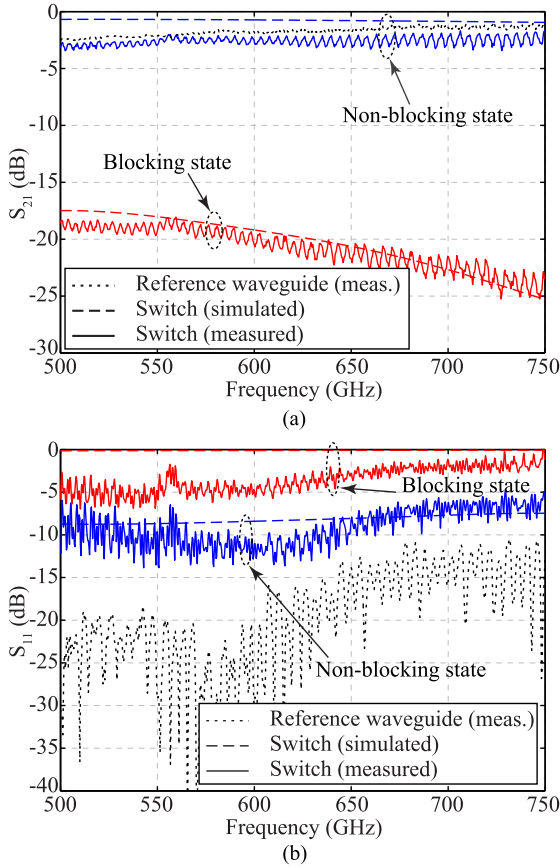


Fig. 8. Measured and simulated S-parameters of the capacitive-contact MEMS waveguide switch with contact overlap of $8 \mu\text{m}$ having five horizontal bars and four vertical columns: (a) S_{21} and (b) S_{11} . The reference waveguide measurement shows the measurement of micromachined hollow straight reference waveguide without any MEMS surfaces.

MEMS waveguide switch design with an $8 \mu\text{m}$ contact overlap having five horizontal bars and four vertical columns. The calibration is done between the two waveguide flanges without any MEMS chip. The broadband frequency measurements between 500 and 750 GHz show that the blocking state isolation (S_{21}) is better than 19 dB and even reaching 24 dB at 750 GHz. This is well matched with the simulation results from CST Microwave Studio where a 200 nm gap between the contacts is used for the blocking state with a simulated insertion loss of 17.5 dB (500 GHz) to 25 dB (750 GHz). The measured insertion loss in the non-blocking state is around 2.2 dB higher when compared to the simulations, which is assumed to be partially attributed to the small gaps in the chip assembly which result in a significant increase in the insertion loss already shown by Shah *et al.* [19]. In addition, the higher insertion loss is also due to limited sidewall gold coverage during sputtering and higher surface roughness during deep reactive ion etching (DRIE) of the $400 \mu\text{m}$ long micromachined waveguide section. This waveguide section is formed by etching the handle layer (thickness = $400 \mu\text{m}$) of the SOI wafer used for fabrication. Using an SOI wafer with a thinner handle layer could improve the insertion loss as shown for the ohmic-contact MEMS waveguide switch where a $300 \mu\text{m}$ SOI handle wafer was used instead. Fig. 9 shows the

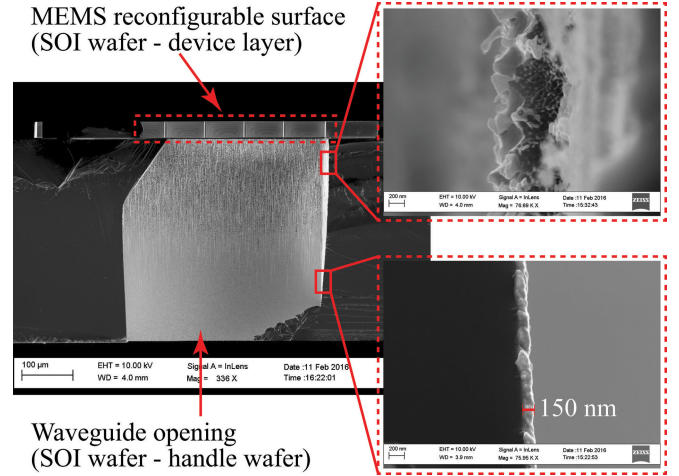


Fig. 9. Cross-sectional SEM image of the fabricated capacitive-contact MEMS waveguide switch with contact overlap of $8 \mu\text{m}$. Close-up of the top and bottom waveguide sidewalls are shown.

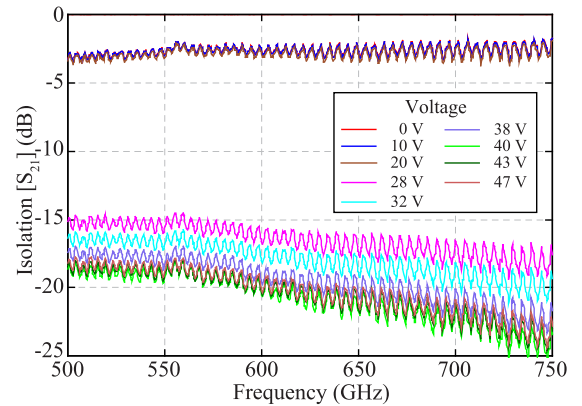


Fig. 10. Measured isolation as a function of actuation voltage for the capacitive-contact MEMS waveguide switch with contact overlap of $8 \mu\text{m}$ having five horizontal bars and four vertical columns.

cross-sectional SEM image of the MEMS waveguide switch chip. The close-up inserts illustrate a uniform metal coverage with a thickness of 150 nm at the top of the micromachined waveguide section and non-uniform metal coverage at the bottom. The higher surface roughness is also clearly visible at larger etch depths of the waveguide section. The contribution to the insertion loss by the MEMS-reconfigurable surface is only about 0.5–1 dB, which is verified by the reference waveguide measurement of a straight micromachined waveguide without the MEMS-reconfigurable surface. The loss factor $(1 - |S_{11}|^2 - |S_{21}|^2)$ for this switch in the blocking state is 0.65 at 500 GHz and going down to 0.3 at 750 GHz. For the non-blocking state, the values are 0.4 at 500 GHz and 0.2 at 750 GHz.

Fig. 10 shows the measured isolation (S_{21}) as a function of actuation voltage for the capacitive-contact MEMS waveguide switch design with an $8 \mu\text{m}$ contact overlap having five horizontal bars and four vertical columns. There is a minimal change in the isolation (S_{21}) when the actuation voltage is increased from 0 to 20 V. From 20 to 28 V, the isolation (S_{21}) increases to

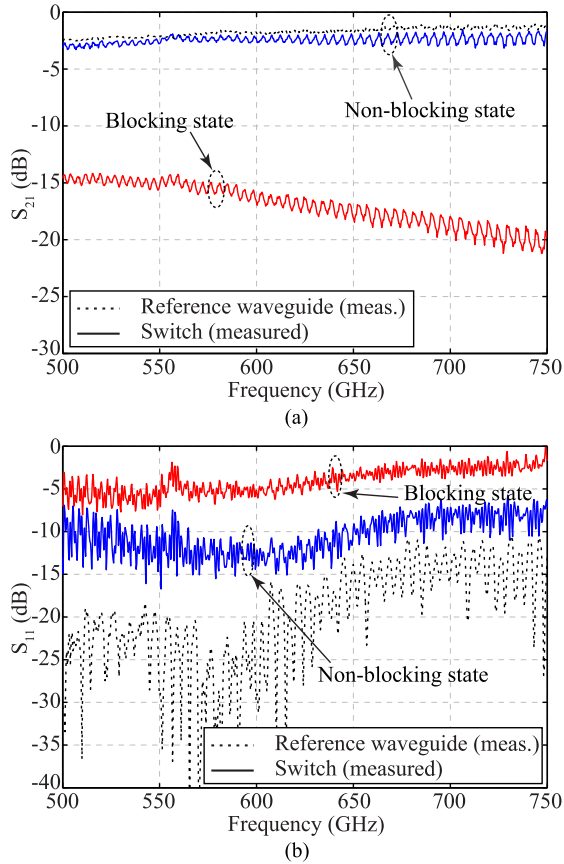


Fig. 11. Measured S-parameters of the capacitive-contact MEMS waveguide switch with contact overlap of $8\ \mu\text{m}$ having five horizontal bars and three vertical columns: (a) S_{21} and (b) S_{11} . The reference waveguide measurement shows the measurement of micromachined hollow straight reference waveguide without any MEMS surfaces.

above 15 dB. At 40 V, the first contact points are touching and any further increase of the actuation voltage does not increase the isolation (S_{21}).

Fig. 11 shows the measured insertion and return loss for a design variation of the capacitive-contact MEMS waveguide switch having five horizontal bars and three vertical columns. The isolation in the blocking state is reduced by around 4 dB when the number of vertical columns is reduced from 4 (see Fig. 8) to 3 (see Fig. 11). This confirms the CST simulations shown in Fig. 3. The improvement in the insertion and return loss in the non-blocking state as predicted by CST simulations in Fig. 3 is not observed in the measurements which is due to the overall losses being dominated by the loss of the $400\ \mu\text{m}$ long micromachined waveguide section. The measured loss factor for this switch in the blocking state is 0.65 at 500 GHz and going down to 0.3 at 750 GHz. For the non-blocking state, the values are 0.4 at 500 GHz and 0.2 at 750 GHz.

2) *Ohmic-Contact Switch*: Fig. 12 shows the simulated and measured insertion and return loss for the ohmic-contact MEMS waveguide switch design with a $2\ \mu\text{m}$ contact cantilever overlap having seven horizontal bars and four vertical columns. The switch has a broadband frequency response with the insertion loss of around 1.2 dB in the non-blocking state for the design

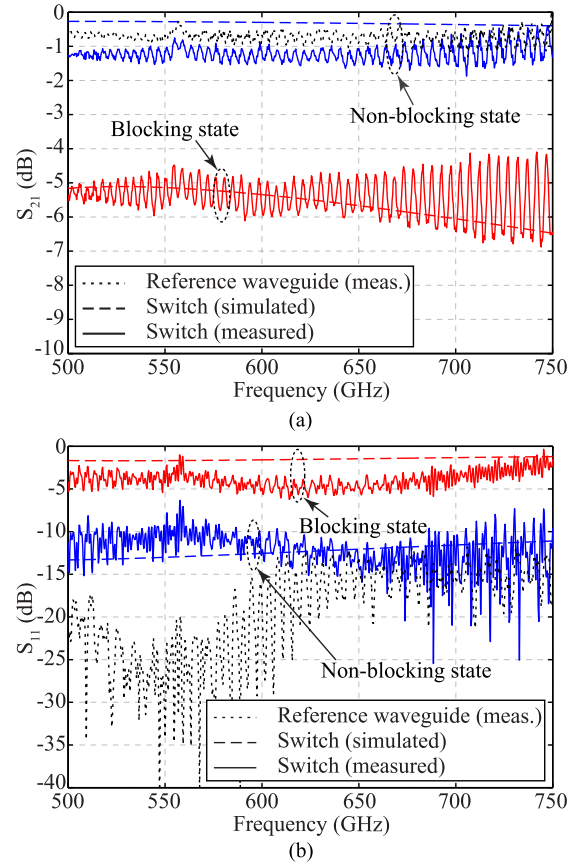


Fig. 12. Measured and simulated S-parameters of the ohmic-contact MEMS waveguide switch with contact overlap of $2\ \mu\text{m}$ having seven horizontal bars and four vertical columns: (a) S_{21} and (b) S_{11} .

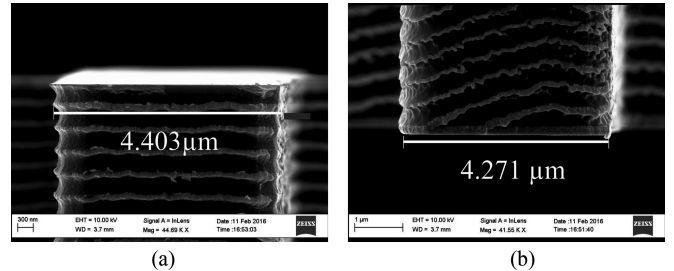


Fig. 13. Cross-sectional SEM image of the contact cantilevers showing a sidewall inclination of 0.25° : (a) top part of the cantilever and (b) bottom part of the cantilever.

frequency range of 500–750 GHz. The measured insertion loss in the non-blocking state is 1.3 dB better than for the capacitive-contact switch (see Fig. 8), which is due to the combination of using a shorter contact cantilever length [see Figs. 2(a) and 3(a)] and the fact that a thinner SOI wafer with handle layer thickness of $300\ \mu\text{m}$ was used in the fabrication. However, the measured switch isolation (S_{21}) in the blocking state is only about 5 dB. This is due to the fabrication irregularities resulting in the decreased probability of all contacts closing which is required for proper operation of the metal-contact switch. Fig. 13 shows fabrication inaccuracies by illustrating the cross-sectional SEM images of the top and bottom part of the contact cantilevers

TABLE I
ACTUATOR DESIGN AND CHARACTERIZATION

Actuator No.	Spring Width [μm]	Gap Between Fingers [μm]	Spring Constant [N/m]	Measured Actuation Voltage [V]
1	3	2	1.06	28
2	3	2.5	1.06	36
3	3.5	2.5	1.69	40
4	4.5	2	3.59	49

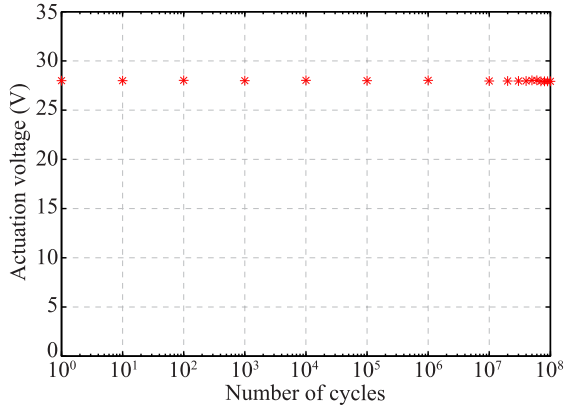


Fig. 14. Life-time measurements with the actuation voltage being monitored over 100 million cycles using a 36 V unipolar square waveform with a 50% duty cycle and a cycle frequency of 100 Hz.

showing a sidewall scallop size of 150–200 nm in the deep reactive ion-etched device layer. In addition, the contact cantilever sidewall profile is not straight and a sidewall angle of 0.25° is measured from the cross-sectional SEM images. To take these fabrication inaccuracies into account in the model, a 200 nm gap between the contact cantilevers was, therefore, used in simulations for the blocking state. The measured loss factor for this switch in the blocking state is 0.3 at 500 GHz and going down to 0.1 at 750 GHz. For the non-blocking state, the values are 0.2 at 500 GHz and 0.1 at 750 GHz.

B. Electromechanical Characterization and Reliability

The design parameters used for the four implemented comb-drive actuators are summarized in Table I together with the measured actuation voltages. Actuator 1 was chosen for further detailed electromechanical characterization. The actuation voltage repeatability measurement shows that for 20 consecutive actuation cycles, the average actuation voltage is 27.99 V with a standard deviation of 44.7 mV.

For performing the lifetime measurements, actuator 1 (see Table I) was cycled using a unipolar square waveform with a 50% duty cycle at a frequency of 100 Hz with an actuation voltage of 36 V (28% overvoltage drive). Fig. 14 shows the result of the lifetime measurements where the actuation voltage was measured after each decade of actuation cycles and remains stable at 28 V with no significant variation over the measured one hundred million cycles (standard deviation of all 45 measurement points is 66.1 mV), performed even in an uncontrolled laboratory environment.

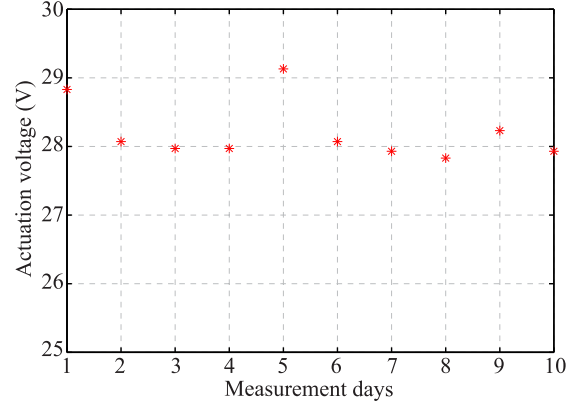


Fig. 15. Long-term continuous actuated state measurements using a voltage of 36 V, with the actuation voltage monitored once per day.

As a further reliability test of the switch design, long-term actuation measurements were performed on actuator 1. The actuator was held in a continuous actuated state for ten days with a voltage of 36 V and only once per day the actuation voltage was measured by averaging the results from three consecutive actuation-voltage ramping cycles at each measurement point. Fig. 15 summarizes the results and shows a very low variation in the measured average actuation voltage over the ten day forced-ON period. The actuator remained fully operational during and after the measurement tests without any sign of failure or degradation.

V. CONCLUSION

We have reported the design, fabrication, and detailed characterization of the first submillimeter-wave 500–750 GHz MEMS waveguide switch comprising a MEMS-reconfigurable surface for blocking/unblocking the wave propagation through a waveguide. Detailed design parameter analysis was performed to select the best design parameters for achieving a low insertion loss in the non-blocking state and a high isolation in the blocking state. Two different switch concepts based on an ohmic-contact and a capacitive-contact between the contact cantilevers were compared. The ohmic-contact waveguide switch did not work properly in the blocking state achieving and isolation of only 5 dB. On the other hand, the capacitive-contact waveguide switch achieved an isolation of 19–24 dB and an insertion loss of 2.5–3 dB, which included losses from a 400 μm long micromachined waveguide section. The major part of the insertion loss is attributed to insufficient gold coverage and surface roughness of the waveguide sidewalls and only 0.5–1 dB is attributed to the MEMS-reconfigurable surface. In addition, lifetime measurements show high actuator reliability at medium actuation voltages, with 100 million cycles and a 10-day down-state test successfully completed.

ACKNOWLEDGMENT

The research described herein is a collaboration effort between the KTH Royal Institute of Technology, Stockholm,

Sweden, and the Jet Propulsion Laboratory, California Institute of Technology, Pasadena, CA, USA, under contract with National Aeronautics and Space Administration.

REFERENCES

- [1] C. A. Leal-Sevillano *et al.*, "Silicon micromachined canonical E-plane and H-plane bandpass filters at the terahertz band," *IEEE Trans. Microw. Wireless Compon. Lett.*, vol. 23, no. 6, pp. 288–290, Jun. 2013.
- [2] W. R. McGrath, C. Walker, M. Yap, and Y.-C. Tai, "Silicon micromachined waveguides for millimeter-wave and submillimeter-wave frequencies," *IEEE Trans. Microw. Guided Wave Lett.*, vol. 3, no. 3, pp. 61–63, Mar. 1993.
- [3] V. M. Lubecke, K. Mizuno, and G. M. Rebeiz, "Micromachining for terahertz applications," *IEEE Trans. Microw. Theory Techn.*, vol. 46, no. 11, pp. 1821–1831, Nov. 1998.
- [4] F. Boussaha, J. Kawamura, J. Stern, and C. Jung-Kubiak, "2.7 THz balanced waveguide HEB mixer," *IEEE Trans. THz Sci. Technol.*, vol. 4, no. 5, pp. 545–551, Sep. 2014.
- [5] COM DEV International, Jul. 1, 2016. [Online]. Available: http://www.meslmicrowave.com/Products_Catalogue/Rotary_Switches/Waveguide_Rotary_Switches.aspx
- [6] Quinstar Technology, Inc., Jul. 1, 2016. [Online]. Available: <http://quinstar.com/millimeter-wave/waveguide-pin-switch-qssqsd-series>
- [7] G. M. Rebeiz, C. D. Patel, S. K. Han, C.-H. Ko, and K. M. J. Ho, "The search for a reliable MEMS switch," *IEEE Microw. Mag.*, vol. 14, no. 1, pp. 57–67, Jan./Feb. 2013.
- [8] H. Zareie and G. M. Rebeiz, "Compact high-power SPST and SP4T RF MEMS metal-contact switches," *IEEE Trans. Microw. Theory Techn.*, vol. 62, no. 2, pp. 297–305, Feb. 2014.
- [9] G. M. Rebeiz, *RF MEMS Theory, Design, and Technology*. New York, NY, USA: Wiley, 2003.
- [10] K. B. Cooper and G. Chattopadhyay, "Submillimeter-wave radar: Solid-state system design and applications," *IEEE Microw. Mag.*, vol. 15, no. 7, pp. 51–67, Nov./Dec. 2014.
- [11] M. Daneshmand and R. R. Mansour, "RF MEMS satellite switch matrices," *IEEE Microw. Mag.*, vol. 12, no. 5, pp. 92–109, Aug. 2011.
- [12] F. Ke, J. Miao, and J. Oberhammer, "A ruthenium-based multimetall-contact RF MEMS switch with a corrugated diaphragm," *J. Microelectromech. Syst.*, vol. 17, no. 6, pp. 1447–1459, Dec. 2008.
- [13] L. Chen, Z. J. Guo, N. Joshi, H. Eid, G. G. Adams, and N. E. McGruer, "An improved SPM-based contact tester for the study of microcontacts," *J. Micromech. Microeng.*, vol. 22, no. 4, Mar. 2012, Art. no. 045017.
- [14] M. Daneshmand, R. R. Mansour, and N. Sarkar, "RF MEMS waveguide switch," *IEEE Trans. Microw. Theory Techn.*, vol. 52, no. 12, pp. 2651–2657, Dec. 2004.
- [15] M. Daneshmand and R. R. Mansour, "Multiport MEMS-based waveguide and coaxial switches," *IEEE Trans. Microw. Theory Techn.*, vol. 53, no. 11, pp. 3531–3537, Nov. 2005.
- [16] N. Vahabisani and M. Daneshmand, "Monolithic millimeter-wave MEMS waveguide switch," *IEEE Trans. Microw. Theory Techn.*, vol. 63, no. 2, pp. 340–351, Feb. 2015.
- [17] Z. Baghchehsaraei, U. Shah, J. Åberg, G. Stemme, and J. Oberhammer, "MEMS reconfigurable millimeter-wave surface for V-band rectangular-waveguide switch," *Int. J. Microw. Wireless Technol.*, vol. 5, no. 3, pp. 341–349, Jun. 2013.
- [18] Z. Baghchehsaraei and J. Oberhammer, "Parameter analysis of millimeter-wave waveguide switch based on a MEMS reconfigurable surface," *IEEE Trans. Microw. Theory Techn.*, vol. 61, no. 12, pp. 4396–4404, Dec. 2013.
- [19] U. Shah *et al.*, "Submillimeter-wave 3.3-bit RF MEMS phase shifter integrated in micromachined waveguide," *IEEE Trans. THz Sci. Technol.*, vol. 6, no. 5, pp. 33–38, Sep. 2016.
- [20] U. Shah *et al.*, "500-750 GHz submillimeter-wave MEMS waveguide switch," in *IEEE MTT-S Int. Microw. Symp. Dig.*, May 2016, pp. 1–4.
- [21] T. Vähä-Heikkilä and M. Ylönen, "G-band distributed microelectromechanical components based on CMOS compatible fabrication," *IEEE Trans. Microw. Theory Techn.*, vol. 56, no. 3, pp. 720–728, Mar. 2008.
- [22] T. J. Reck, C. Jung-Kubiak, and G. Chattopadhyay, "A 700-GHz MEMS waveguide switch," *IEEE Trans. THz Sci. Technol.*, vol. 6, no. 4, pp. 641–643, Jul. 2016.
- [23] T. J. Reck, C. Jung-Kubiak, J. Gill, and G. Chattopadhyay, "Measurement of silicon micromachined waveguide components at 500-750 GHz," *IEEE Trans. THz Sci. Technol.*, vol. 4, no. 1, pp. 33–38, Jan. 2014.



Umer Shah (S'09–M'14) was born in Bannu, Pakistan, in 1981. He received the B.S. degree in engineering from the Ghulam Ishaq Khan Institute of Engineering Sciences and Technology, Topi, Pakistan, in 2003, the M.Sc. degree in wireless engineering from the Technical University of Denmark, Kgs. Lyngby, Denmark, in 2007, and the Ph.D. degree in microsystem technology from the KTH Royal Institute of Technology, Stockholm, Sweden, in 2014.

Since May 2014, he has been a Postdoctoral Researcher with the Micro and Nanosystems Group, KTH Royal Institute of Technology. He has authored or co-authored more than 30 reviewed works as the recipient of papers. His research focuses on RF MEMS-based filters, phase shifters, matching circuits, and antennas.

Dr. Shah was the recipient of the Best Student Paper Award presented at the Asia-Pacific Microwave Conference 2010, Yokohama, Japan. He was also the recipient of the 2014 IEEE MTT-S Graduate Fellowship Award for his research activities.



Theodore Reck (M'04–SM'15) received the B.S. degree in electrical engineering from The University of Texas at Austin, Austin, TX, USA, in 2000, and the Ph.D. degree in electrical engineering from the University of Virginia, Charlottesville, VA, USA, in 2010.

From 2010 to 2013, he was a NASA Postdoctoral Fellow with the Jet Propulsion Laboratory (JPL), Pasadena, CA, USA, designing terahertz devices that utilize silicon micromachining. He is currently a Member of the Technical Staff with the JPL. His research interests also include RF-MEMS, antenna arrays, terahertz metrology, and cryogenic MMIC LNAs.



Henrik Frid (S'13) received the B.Sc. and M.Sc. degrees in engineering physics (with a specialization in electromagnetic theory, antenna theory, and electromagnetic wave propagation and scattering) from the KTH Royal Institute of Technology, Stockholm, Sweden, in 2014. He is currently working toward the Ph.D. degree in electrical engineering at the KTH Royal Institute of Technology.

Parallel to his studies, he was a Research Assistant with KTH on the topic of electrohydrodynamic flow simulations for liquid high-voltage insulators. During 2013, he joined Saab, Linköping, Sweden, for an internship on polarimetric radar calibration, and in 2014, he did a M.Sc. thesis project with Saab, Järfälla, Sweden, on calculating the mutual coupling between antennas on an aircraft. His current research interests include electromagnetic theory, reconfigurable antennas, and RF-THz MEMS-based switches and antennas.

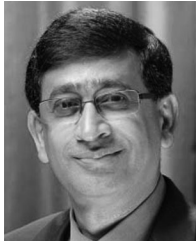
Mr. Frid was the recipient of the 2012 Multiphysics Student Award and was selected for the 2014 Excellence Doctoral Program at KTH.



Cecile Jung-Kubiak (M'15) received the Master's degree in physics and materials chemistry from Polytech Montpellier, Montpellier, France, in 2006, and the Ph.D. degree in physics from Université Paris-Sud XI, Orsay, France, in 2009.

She received a two-year NASA Postdoctoral Fellowship with the California Institute of Technology, in 2010. She is currently a Member of the Technical Staff with the S.W.A.T. Group, Jet Propulsion Laboratory (JPL), Pasadena, CA, USA. She has co-authored more than 50 papers in international journals and conferences and holds several patents. Her research interests include the development of silicon micromachining technologies using DRIE techniques, the miniaturization of multipixel arrays to build compact 3-D instruments, and GaAs-based frequency multipliers and mixers in the THz region.

Dr. Jung-Kubiak was the recipient of the 2010 JPL Outstanding Postdoctoral Research Award in Field Technology, Instrumentation, and Engineering and the 2014 IEEE THz Science and Technology Best Paper Award.



Goutam Chattopadhyay (S'93–M'99–SM'01–F'11) received the B.E. degree in electronics and telecommunication engineering from the Bengal Engineering College, Calcutta University, Calcutta, India, in 1987, the M.S. degree in electrical engineering from the University of Virginia, Charlottesville, VA, USA, in 1994, and the Ph.D. degree in electrical engineering from the California Institute of Technology (Caltech), Pasadena, CA, USA, in 1999.

He is a Senior Research Scientist with NASA's Jet Propulsion Laboratory, and a Visiting Associate with the Division of Physics, Mathematics, and Astronomy, Caltech. From 1987 to 1992, he was a Design Engineer with the Tata Institute of Fundamental Research, Pune, India. He has authored or co-authored more than 250 publications in international journals and conferences and holds more than 15 patents. His research interests include microwave, millimeter-, and submillimeter-wave heterodyne and direct detector receivers, frequency sources and mixers in the terahertz region, antennas, SIS mixer technology, direct detector bolometer instruments; InP HEMT amplifiers, mixers, and multipliers; high-frequency radars, and applications of nanotechnology at terahertz frequencies.

Dr. Chattopadhyay was the recipient of numerous awards and honors including, the Best Undergraduate Student Award from the University of Calcutta in 1987, the Jawaharlal Nehru Fellowship Award from the Government of India in 1992, and the IEEE MTT-S Graduate Fellowship Award in 1997. He was the recipient of the Best Journal Paper Award in 2013 of the IEEE TRANSACTIONS ON TERAHERTZ SCIENCE AND TECHNOLOGY, and the IETE Prof. S. N. Mitra Memorial Award in 2014. He was also the recipient of more than 30 NASA Technical Achievement and New Technology Invention Awards. He is an Associate Editor of the IEEE TRANSACTIONS ON ANTENNAS AND PROPAGATION, a Fellow of the IETE (India), and an IEEE Distinguished Lecturer.



Imran Mehdi (S'83–M'90–SM'05–F'10) received the B.S.E.E., M.S.E.E., and Ph.D. degrees from the University of Michigan, Ann Arbor, MI, USA, in 1985, 1986, and 1990, respectively.

He is a Senior Research Scientist with the Jet Propulsion Laboratory (JPL), California Institute of Technology, Pasadena, CA, USA. He joined the JPL in 1990 and is currently a Group Supervisor with the Instrument Electronics and Sensors Section. His responsibilities include developing THz components, technologies, and subsystems for current and future

NASA missions. These devices and components were implemented on the ozone monitoring microwave limb sounder instrument, which is still operational, as well as the (Microwave Instrument on Rosetta Orbiter) MIRO instrument, which represents the first submillimeter-wave receiver operational in deep space. From 1999, he led the effort of developing broadband solid-state sources from 200 to 2500 GHz for the Heterodyne Instrument for Far Infrared (HIFI) on the Herschel Space Observatory, a cornerstone European Space Agency mission. HIFI has successfully completed its mission enabling ground-breaking astrophysics observations. His current interests include millimeter and submillimeter-wave devices and technology, nanotechnology, high-frequency instrumentation, 3-D submm-wave systems, and development of compact low-power heterodyne receivers for planetary missions.

Dr. Mehdi is a Topical Editor for the IEEE TRANSACTIONS ON TERAHERTZ SCIENCE AND TECHNOLOGY.



Joachim Oberhammer (M'06–SM'12) was born in Brunico, Italy, in 1976. He received the M.Sc. degree in electrical engineering from the Graz University of Technology, Graz, Austria, in 2000, and the Ph.D. degree from the KTH Royal Institute of Technology, Stockholm, Sweden, in 2004.

He was a Postdoctoral Research Fellow with Nanyang Technological University, Singapore, in 2004, and with Kyoto University, Japan, in 2008. Since 2005, he has been leading radio-frequency/microwave/terahertz microelectromechanical systems research at KTH; an Associate Professor with KTH since 2010; and a Professor in microwave and THz microsystems with KTH since 2015. He was a Guest Researcher with Nanyang Technological University, in 2007 and with the NASA Jet Propulsion Laboratory, Pasadena, CA, USA, in 2014. He has authored or co-authored more than 100 reviewed research papers and holds 4 patents.

Dr. Oberhammer was the recipient of an award by the Ericsson Research Foundation, a grant by the Swedish Innovation Bridge, and a scholarship by the Japanese Society for the Promotion of Science, in 2004, 2007, and 2008, respectively. The research work he is heading received six Best Paper Awards (five of which at IEEE conferences) and four IEEE Graduate Fellowship Awards (by the IEEE MTT-S and by AP-S) since 2009. He served as a TPRC member of IEEE Transducers 2009 and 2015, the IEEE International Microwave Symposia 2010–2016, IEEE Micro Electro Mechanical Systems 2011 and 2012, and IEEE Radio and Wireless Week 2015 and 2016. He has been a Steering Group member of the IEEE MTT-S and AP-S Chapters Sweden since 2009. In 2013, he received an ERC Consolidator Grant by the European Research Council. Since 2014, he has been a Steering Group member of the Young Academy of Sweden.